

Pulsed eddy current empirical modeling

J.H.V. Lefebvre⁽¹⁾, C. Mandache⁽²⁾, J. Letarte⁽¹⁾

⁽¹⁾*Air Vehicles Research Section, Defence R&D Canada, Ontario, Canada, K1A 0K2;* ⁽²⁾ *NRC / Institute for Aerospace Research, 1200 Montreal Road, Building M14, Ottawa, Ontario, Canada, K1A 0R6.*

Abstract

The pulsed eddy current responses to varying material thickness and conductivity are modeled using an electrical circuit ideal transformer non-linear model. The Levenberg-Marquardt algorithm is used to curve fit the experimental signal to the model. The resulting synthetic signal is examined for its ability to preserve experimental signal features such as lift-off point of intersection (LOI), a pulsed eddy current signal feature used successfully in NDE of corrosion, cracks, thickness and conductivity measurements. The method is tested on specimens for its ability to reproduce inspection images using synthetic signals in lieu of experimental signals. This procedure conserves data storage space and allows rapid analysis of images using equations.

Keywords: pulsed eddy current, Levenberg-Marquardt, bootstrap, curve fitting, lift-off

1. Introduction

The signal obtained during conventional eddy current testing ranges from simple curves in the impedance plane diagram to more complex lemniscates. The obtained signal depends on the type of transducer used, the material under inspection, its discontinuities, and the frequency of excitation. There have been many attempts to model conventional eddy current signal patterns using Fourier descriptors [1,2,3]. The objective was to characterize the signal patterns with a few parameters so that signal storage space could be reduced. Some issues were (1) the ability to reproduce the original signal with high fidelity, (2) using a set of parameters capable of providing an intuitive understanding of the physical phenomena, (3) a different and unique set of parameters for different discontinuities, and (4) the ability to allow automatic discontinuity recognition [1]. Dodd and Deeds explored the equivalent work for pulsed eddy current within a general theoretical framework for polynomial approximation [4,5]. This multi-parameter polynomial method allowed material property recognition with good accuracy, providing the proper points were selected in the experimental signal. The ability to reproduce the signal with minimal data storage and high fidelity was not explored. The uniqueness of parameters to the material condition was also not determined.

In this study, the non-linear response of a single absolute coil transducer is fitted to an electrical circuit equivalent model (*figure 1.a*). The resulting model is then used to simulate pulsed eddy current inspection of simple structures. The Levenberg-Marquardt (LM) curve-fitting algorithm for non-linear models is used [7,8]. The quality of the curve fitting is verified by means of visual observation and residuals comparison of the experimental curve to the synthetic curve generated using the parameters. The parameters' stability to small changes in the data due to noise is tested using a bootstrap algorithm. The model's ability to reproduce with high fidelity the experimental signal is further tested by comparing the lift-off point of intersection (LOI) obtained experimentally and synthetically under various test conditions. It is a requirement of this work that the LOI be retained as it is a pulsed eddy current feature used for evaluation of corrosion, for cracks, and for multi-layer structures inspection [6]. The method is lastly verified by comparing a test article image constructed with experimental signals to that of an image constructed with synthetic data.

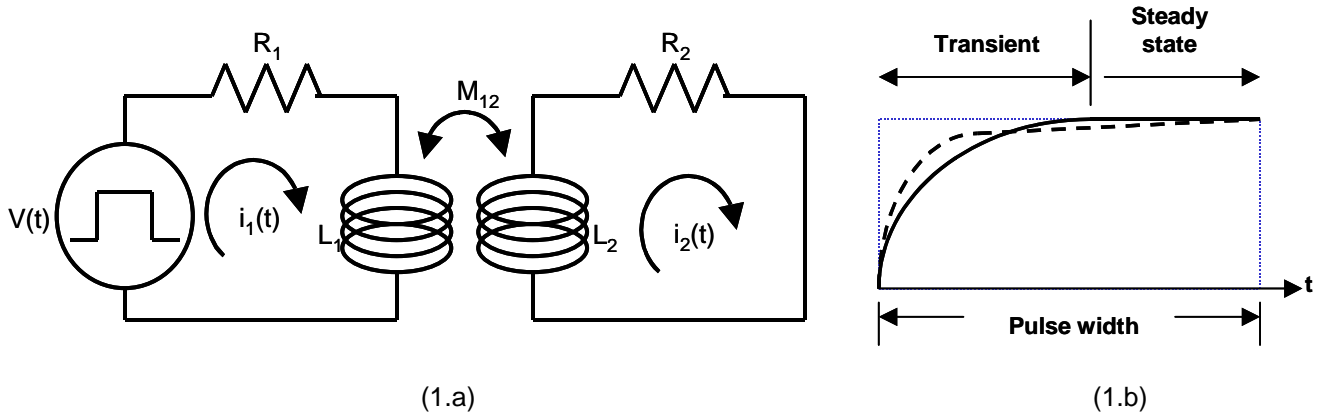


Figure 1. Circuit equivalent model. (1.a) The transducer is represented by a resistance (R_1) and an inductance (L_1). It is coupled by a mutual inductance (M_{12}) to the specimen represented by a resistance (R_2) and an inductance (L_2). (1.b) Signal when exposed to air (full line) and signal when exposed to a conductor (dotted line).

2. Non-linear curve fitting algorithm

A recognized non-linear least-square fitting method is the LM algorithm [7]. This algorithm uses information in the gradient and Hessian matrices to find an approximate distance and direction to the nearest minimum from the starting values [8]. The LM algorithm requires (i) a model, represented by an equation with n parameters, to which to fit the experimental data, (ii) the n partial derivatives with respect to the n parameters, and (iii) adequate initial guess values. This provides a problem with $n+1$ equations to find n parameters.

2.1 Circuit equivalent model. A circuit equivalent model commonly used to represent the physical eddy current test is the ideal transformer [9]. It provides a first order approximation capable of describing the signal response behaviour. *Figure (1.a)* represents the ideal case under a pulsed excitation, $V(t)$. A resistance (R_1) in series with an inductance (L_1) represents a single coil transducer electrical properties. A resistance (R_2) in series with an inductance (L_2) represents the specimen's electrical properties. The transducer and the specimen are coupled by the mutual inductance (M_{12}) a function of the coupling factor (k). Under this arrangement the current in the transducer, $i_1(t)$, will vary with varying test article conditions. A set of coupled differential equations (1) represents this situation. If the transducer is exposed to air (a non-conductor) equation (1) is simplified by equating R_2 , L_2 , and M_{12} to zero. The solutions to equations (1) when the transducer is exposed to air or a conductor can be solved using Laplace transforms, the solutions of which are widely available in literature [10].

$$\begin{aligned}
 V(t) &= R_1 i_1(t) + L_1 \frac{di_1(t)}{dt} - M_{12} \frac{di_2(t)}{dt} \\
 0 &= R_2 i_2(t) + L_2 \frac{di_2(t)}{dt} - M_{12} \frac{di_1(t)}{dt} \\
 M_{12} &= L_1 L_2 k^2
 \end{aligned}
 \tag{1}$$

In the case of the transducer in air, the solution for the current in the transducer has the form given by equation (2). In the case of the transducer near a conductor, the solution for the current in the transducer has the form given by equation (3). Given that the current in the transducer is measured indirectly as a voltage across a resistance, or as a voltage through a voltage-follower, and that the entire test set-up electrical properties are not taken into account, the precise formulations in term of

resistance and inductance for the parameters A , a , B , b , C , c or D are not of interest. Only the general shape of the equations and number of parameters in (2) and (3) are of interest.

$$e(t) = A - Ae^{at}, \quad a = \frac{\ln(1 - e(t)/A)}{t} \quad (2)$$

$$f(t) = Be^{bt} + Ce^{ct} + D \quad (3)$$

2.2 Associated differential equations. Differentiating equations (3), with respect to the parameters, for the case of the transducer exposed to a conductor provides equations (4). Equations (3) and (4) form the complete set of equations required by the LM algorithm.

$$\begin{aligned} \frac{\partial f(t)}{\partial B} &= e^{bt} & \frac{\partial f(t)}{\partial b} &= Bte^{bt} & \frac{\partial f(t)}{\partial C} &= e^{ct} \\ \frac{\partial f(t)}{\partial c} &= Cte^{ct} & \frac{\partial f(t)}{\partial D} &= 1 \end{aligned} \quad (4)$$

2.3 Initial guess values. With the LM algorithm, choosing adequate initial guess values is a crucial constraint. The starting parameter values need to be as close as possible to final parameters values in order to avoid being trapped in a local minimum or not converging to a solution. This is especially critical when the number of parameters to be fitted is high [7,8]. In this study, two sets of initial guess values are provided. The first set of initial guess values is provided by using the parameters A and a of the transducer signal in air. The subsequent sets of initial guess values are provided using the parameters B , b , C , c and D found in a previous curve fitting of the transducer response when exposed to the test article. The rationale for this is as follows. It is observed experimentally that the transducer's response when exposed to air is very similar to that of a transducer exposed to a conductive test article (*figure 1.b*). Yet, equation (2) representing the air exposure situation is relatively simple and its parameters A and a can be easily estimated. Parameter A is estimated as the mean steady state value of the signal. Once parameter A is available, equation (2) can be linearized and the value of parameter a is found by least-square approximation. The value estimated for A as amplitude is then used as the first initial guess for B , C , and D amplitudes. The value of the exponent a is used for the exponents b and c as the first initial guess values in the LM algorithm. The second stage for providing close initial guess values involves simply using the parameters B , b , C , c , and D from a previous curve fitting. The reason for this being that the parameters found from the previous curve fitting process would always be very close to the new parameters. This allows automatic and rapid curve fitting for a C-scanned specimen. The curve fitting process described above was tried using previously published results with a single coil probe [6]. Sets of titanium (3.5 percent of International Annealed Copper Standard, %IACS), brass (26.5 %IACS), aluminum (59.5 %IACS) and copper (100.1 %IACS) shims and plates of various thickness were used to provide a wide spectrum of thickness and conductivity effects on the probe's response. Conductivity standards (1, 3, 9, 29, 32, 38, 42, 48, 59, 87 and 100 %IACS) were also used to evaluate the effect of conductivity only. The response at design lift-off and three different applied lift-offs were recorded for all test conditions. This experiment provided approximately 130 single coil transducer responses to test the curve fitting process.

3. Results

3.1 Visual and Residuals. A typical direct visual comparison of the experimental responses and the synthetically generated curves is shown in *figure 2.a*. Both curves overlap with excellent fit. However, important, yet minute, differences can still be present but hidden by the scale used. By showing the difference between the experimental and synthetic curves in relative percentage terms, these minute differences are enhanced. The relative residuals for the typical curves are shown in *figure 3.b*. The

relative difference between the experimental curve and the synthetic curve did not exceed 0.3% in most regions of the curve. The exceptions always being relatively large discrepancies during the first 2 to 3 μs that represent about 4% of the recorded response. This is discussed later in section 3.5. Overall, the fit between experimental and synthetic curves proved to be excellent.

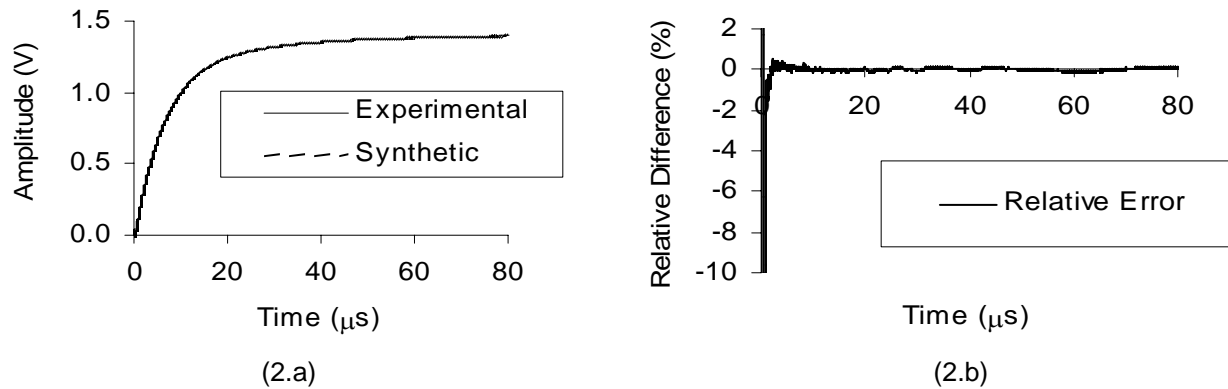


Figure 2. Typical curve fitting results. (2.a) Overlapping experimental and synthetic curves, (2.b) relative difference between experimental and synthetic curves.

3.2 Stability. One issue of concern is the stability of the parameters under varying noise. If small changes in noise induce high variations in parameter values then the parameters may not be reproducible and pattern recognition impossible. To test the parameter stability, it was decided to use a bootstrap algorithm to generate synthetic sets of data from which new synthetic parameters would be obtained [7]. The bootstrap was performed 20 times to obtain a mean parameter and a standard deviation. The curve fitting process was deemed stable if (i) the bootstrap standard deviation was within $\pm 5\%$ of the mean bootstrap parameter found and if (ii) the mean bootstrap parameter agreed within $\pm 5\%$ of the original curve fitting parameters found. All parameters were compared against these two criteria. Adherence to the first criterion was evaluated by taking the ratio of the bootstrap standard deviation to its bootstrap mean parameter. Adherence to the second criterion was evaluated using the ratio of the original curve fitting parameter value to the bootstrap parameter value. This was repeated for all parameters and for all signals that were curve fitted. To ease the evaluation, all ratios obtained were plotted in *figure 3*, where the semi-circle represents the $\pm 5\%$ criteria. It is to be noted that most points fall in a small cluster well inside the semi-circle. With a few exceptions, the curve fitting process proved to be very stable showing only small variations in the parameter values when subjected to varying noise. This is indicative of a very stable curve fitting process. Again exceptions are observed and are explained in section 3.5.

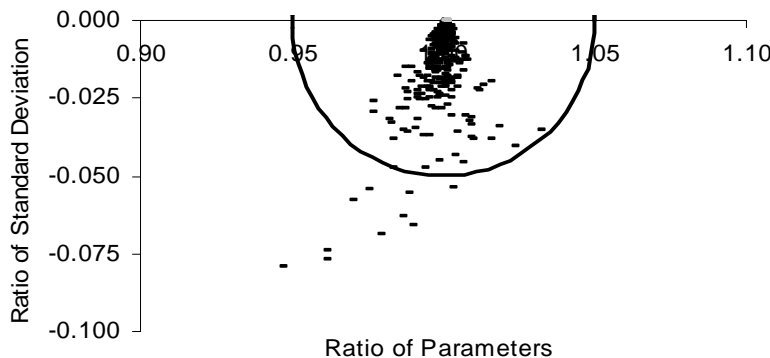


Figure 3. Parameter Stability

3.3 LOI feature. The LOI is a feature used to provide an evaluation independent of lift-off in pulse eddy current. Therefore, it is very important to preserve it in the curve fitting process. *Figure 4.a* shows two typical experimental signals taken at different lift-offs but identical test article condition. Their synthetic curves are also shown. It can be seen intuitively from *figure 4.a*, that the LOI feature is preserved in that all four signals cross each other at the same location. This can be amplified by subtracting the experimental signals one from another and likewise for the synthetic curves. *Figure 4.b* shows that the differences provide the same zero amplitude crossing time near 22 μs . The ability of the curve fitting process to preserve the LOI time-amplitude coordinates was verified for all test conditions and good agreement was obtained.

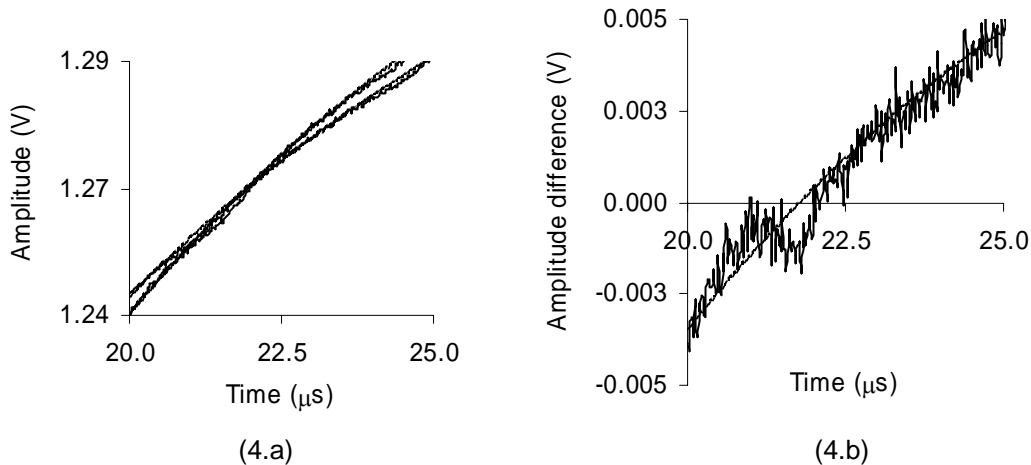


Figure 4. LOI feature preservation. (4.a) close-up view of two experimental signals with varying lift-off only, (4.b) close-up view of the difference between the two signal showing that experimental and synthetic curve subtraction provide the same LOI time.

3.4 Imaging. The curve fitting process was also used tested by comparing an experimental image and a synthetic image. The data was obtained by scanning a 1.025 mm thick aluminum specimen with a 10 mm radius circularly-shaped bottom side material loss of 35%. The top surface was covered with varying layers of non-conducting tape to simulate varying lift-off effects of 0 mm, 0.115 mm and 0.230 mm. The experimental and synthetic amplitudes results at LOI time are shown side by side in *figure 5*. It can be seen that there is no loss of information from the synthetic data.

3.5 Limitations. In sections 3.1, 3.2 and 3.3 exceptions to the general good fit of the process used here were noted. For all signals, the first 2 to 3 μs showed some discrepancy between the experimental data and the synthetic curve. The problem may be due to an impedance mismatch and ringing or the trigger delay between the start of the signal recording and the pulse generation not being fully accounted for. However the early discrepancy did not affect the overall results. The parameter stability and LOI feature preservation also showed some problem areas. Under close examination, the exceptions to the stability and LOI feature preservation were confined to a few samples. It was noticed that for very thin samples or not so thin very low conductivity samples, the experimental signal varied little with varying lift-off or even from the transducer response when exposed to air. Furthermore, noise levels prevented differentiation of some test article variations. For those specimens, the transducer was operating at or beyond its own limitations. Under those circumstances, the curve fitting process still provided an overall good fit but the parameters became unstable.

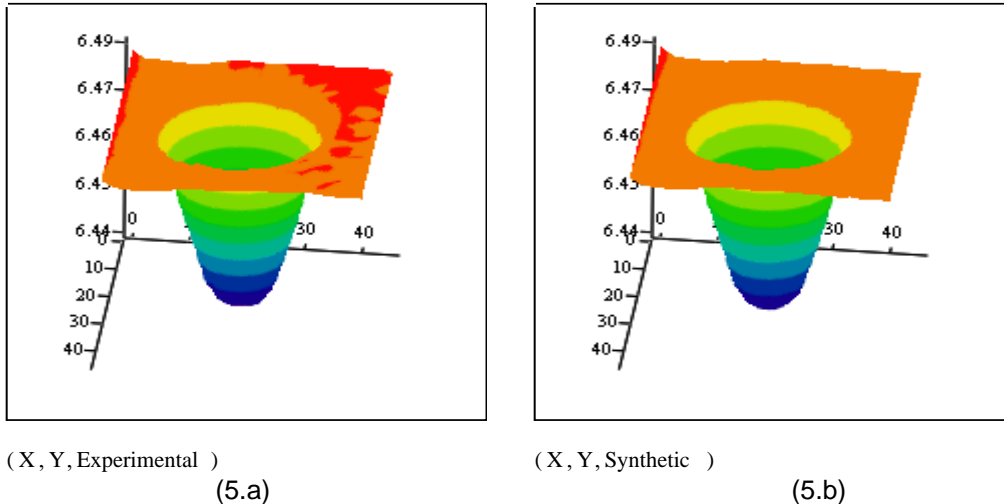


Figure 5: Image reconstruction. The experimental image (5.a) information is preserved in the synthetic image (5.b).

4. Conclusion and future work

A simple process to curve-fit pulsed eddy current signals using the Levenberg-Marquardt algorithm and the ideal transformer model was presented here. The process is capable of providing an excellent fit between experimental and synthetic curves. The curve fitting process is shown to provide stable parameters under noise variation. It has also the ability to preserve key signal features such as the LOI time-amplitude coordinates and the LOI behaviour. The curve fitting process is, however, limited to the operating regime of the transducer. Future work will consist of adapting and testing the curve fitting process with other models of transducer. The synthetic results will also be explored to extract more information from the signal.

REFERENCES

- [1] Lord (W.), Satish (S.R.), *Fourier descriptor classification of differential eddy current probe impedance plane trajectories*, Progress in Quantitative Nondestructive Evaluation, 1982, vol 3, pp 589-603.
- [2] Udpa (S.S.), *An efficient technique for storing eddy current signals*, Progress in Quantitative Nondestructive Evaluation, 1987, vol 6, pp 855-862.
- [3] Stepinski (T.), *Analysis of eddy current patterns review and recent results*, Progress in Quantitative Nondestructive Evaluation, 1991, vol 10, pp 943-950.
- [4] Deeds (W.E.), Dood (C.V.), *Determination of multiple properties with multiple eddy current measurements*, International Advances in Nondestructive Testing, 1981, vol 8, pp 317-333.
- [5] Dood (C.V.), Deeds (W.E.), *Multiparameter methods with pulsed eddy currents*, Progress in Quantitative Nondestructive Evaluation, 1987, vol 6, pp 849-854.
- [6] Lefebvre (JHV) and Dubois (S) , *Lift-Off point of Intersect (LOI) behaviour*, Progress in Quantitative Nondestructive Evaluation, 2005, vol 24, pp 523-530.
- [7] Press (WH) and al, *Numerical recipes in C++*, Cambridge University press, 2002.
- [8] Bevington (P.R.), Robinson (D.K.), *Data Reduction and Error Analysis for the Physical Sciences*, McGraw-Hill, 1992.
- [9] Libby, (H.L.), *Introduction to electromagnetic nondestructive Test Methods*, Wiley-Interscience, New York ,1971.
- [10] Kreysig (E), *Advanced Engineering Mathematics*, Ed Wiley, New York, 3rd Edition, 1972.

Automated Pulsed Eddy Current Method for Detection and Classification of Hidden Corrosion

M. S. Safizadeh, Z. Liu, C. Mandache, D. S. Forsyth, and A. Fahr

*Structures, Materials & Propulsion Laboratory, Institute for Aerospace Research,
National Research Council Canada, Building M-14, 1200 Montreal Rd.,
Ottawa, Ontario, Canada*

Abstract

Corrosion has an important effect on the structural integrity of aging aircraft components, and an automatic and effective method of corrosion detection and classification can help to ensure the safe operation of a transportation system. Pulsed eddy current (PEC) has been shown to effectively characterize hidden corrosion in aircraft fuselage lap joints. However, two noise sources in the form of probe lift-off and interlayer gap can cause false indications or inaccuracies in quantification.

This paper describes the development of a modular architecture for analysis of PEC data to enable automatic characterization of hidden corrosion in a typical aircraft fuselage multi-layer structure. The goal of this study was to develop a software tool to detect and distinguish between first layer and second layer corrosion damage.

This investigation is a follow on to previous work that applied time-frequency analysis of PEC signals to provide specific visual patterns related to the interlayer gap, lift-off, and material loss. In the present work, the authors have investigated the time-frequency analysis of PEC signals along with feature extraction and classification to automatically characterize and determine the location of material loss in a two-layer structure.

1. Introduction:

Recent advances in the pulsed eddy current technique have shown the potential to detect and characterise hidden corrosion in multi-layer aircraft structures such as lap splices [1,2].

In PEC, the probe's driving coil is excited by repeated pulses. For every pulse, the response signal is measured with a sensor, which may be the driving coil, another

coil, or a Hall or GMR sensor. By sampling the time-domain response using a high-speed digitiser, the probe response is effectively captured over a wide range of frequencies within a single measurement. This allows inspection of the entire depth of the specimen with just one pulse.

The most common features used in the analysis of PEC signals for detection and characterization of material loss due to corrosion in multi-layer structures are the amplitude, time-to-peak or time-to zero-crossing. However, these features are not sufficient for discriminating signals due to corrosion –induced metal loss from unwanted noise. Two of the most important noise sources in lap joint inspections are the variation in probe lift-off and interlayer gap due to change in paint or adhesive thickness, and corrosion pillowing. Previous work of the authors [3] has shown that the time-frequency analysis of pulsed eddy current signals provides visual discrimination between the simultaneous occurrence of material loss and changes in interlayer gap or lift-off. However, this method cannot currently be readily used because of difficulties in calibration and the lack of an automatic detection and classification system.

This paper presents an automated pulsed eddy current method capable of detecting and classifying the material loss due to corrosion, and determining its location in a two-layer structure.

2. Principal of method:

Conventional pulsed eddy current techniques for corrosion detection and characterization rely on the analysis of signal features that are represented as c-scan images. Only experienced operators are able to perform full evaluation of pulsed eddy current c-scan images. Increasing emphasis on reliability and demand for tools that can assist operators have motivated research for an automated pulsed eddy current detection and classification system.

The automatic pulsed eddy current detection and classification system developed in this work includes three modules: a time-frequency analysis module, feature extraction module, and classification module; as shown in Figure 1.

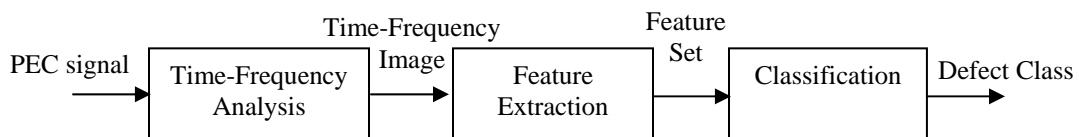


Figure 1: Modular architecture for the proposed pulsed eddy current system.

Details about each module are described in the following.

2.1. Time-Frequency Module

Time-frequency analysis provides a three-dimensional representation of signals in time-frequency-amplitude space, but usually, the projection of this three-dimensional representation is shown in the two-dimensional time-frequency plane with grey scale representing the amplitude.

There are several possible time-frequency distributions; however, we will focus only on the Wigner-Ville distribution (WVD) that is most commonly used.

The Wigner-Ville distribution of a signal $s(t)$ is defined as [4]:

$$WVD_s(t, \omega) = \int_{-\infty}^{\infty} s(t + \tau/2) s^*(t - \tau/2) e^{-j\omega\tau} d\tau \quad (1)$$

where $s(t)$ is a continuous complex signal, τ is a time shift variable and the asterisk denotes the complex conjugation. The discrete-time and discrete-frequency version of equation (1) is given by [5]:

$$WVD_s(n, \pi m / M) = 2 \sum_{k=-M/2+1}^{M/2} p(k) s(n+k) s^*(n-k) \exp(-j2\pi mk / M) \quad (2)$$

$$m = 0, 1, 2, \dots, M-1$$

where $p(k)$ is the window function such as Hamming, Hanning, or rectangle with the length M centred about n .

The WVD has a number of desirable mathematical properties such as time and frequency marginal conditions, instantaneous frequency, time shift, frequency shift, and time and frequency support properties. Despite the desirable properties of the WVD, it has two major draw-backs: it is not necessarily non-negative and it is a bilinear function producing interferences or cross terms for multi-component signals. In practical applications, the WVD requires some smoothing in order to suppress the cross terms.

2.2. Feature Extraction Module

Feature extraction is crucial for pattern recognition systems. The number of features determines the measurement cost and a well-defined feature set plays an important role in the accuracy and efficiency of the subsequent processing.

The output of the time-frequency analysis module is the WVD representation of the pulsed eddy current signals, which are images with a large amount of redundant information. To improve computational efficiency, it is vital to reduce the number of parameters (inputs) in the classifier. Two different feature extractors are used and compared in this study.

One well known linear feature extractor is principal component analysis (PCA) [6]. PCA is a method of identifying patterns in data (the time-frequency images of the PEC signals in our case), and expressing the data in such a way as to highlight their similarities and differences.

PCA computes the m largest eigenvectors of the $d \times d$ covariance matrix of the $n \times d$ -dimensional patterns. The linear transformation is defined as:

$$Y = HX \quad (3)$$

where X is the given $n \times d$ pattern matrix, Y is the derived $n \times m$ ($m < d$) pattern matrix, and H is the $d \times m$ matrix of linear transformation whose columns are the eigenvectors. Since PCA only retains the most expressive features (eigenvectors with the largest eigenvalues), it effectively reduces the number of dimensions without much loss of information.

Let each WVD image be a $N \times N$ matrix. This matrix can be expressed as a N^2 -dimensional vector where the rows of pixels in the image are placed one after the other to form a one-dimensional image.

$$WVD = (w_{11} w_{12} \dots w_{1N} w_{21} \dots w_{NN}) \quad (4)$$

The values in the vector are the intensity values of the image, possibly a single greyscale value. All the WVD image vectors are then put in one matrix:

$$X = \begin{pmatrix} \text{Image Vector 1} \\ \text{Image Vector 2} \\ \vdots \\ \text{Image Vector n} \end{pmatrix} \quad (5)$$

which gives us a starting point for our PCA analysis. Since all the vectors are N^2 dimensional, we will get N^2 eigenvectors. Once we have performed PCA, we obtain the original data mapped into the axis corresponding to the eigenvectors. In practice, we are able to leave out some less significant eigenvectors. In our case, two eigenvectors that correspond to the two largest eigenvalues are chosen for investigation. This choice of eigenvectors permits a visual examination of the data.

Another feature extractor which has been examined is the moments in time and frequency of a time-frequency representation. Since the time-frequency image describes the evolution with time of the frequency content of the signal, the extraction of information has to be done with care from the knowledge of these properties. The first order moments of a Wigner-Ville distribution in time and in frequency are defined as:

$$\begin{aligned} \langle \omega \rangle_t &= \frac{\int_{-\infty}^{+\infty} \omega WVD(t, \omega) d\omega}{\int_{-\infty}^{+\infty} WVD(t, \omega) d\omega} \\ \langle t \rangle_\omega &= \frac{\int_{-\infty}^{+\infty} t WVD(t, \omega) dt}{\int_{-\infty}^{+\infty} WVD(t, \omega) dt} \end{aligned} \quad (6)$$

Equation 6 describes the averaged position and spread in time and frequency of the signal. For a Wigner-Ville distribution, the first order moment in time also corresponds to the instantaneous frequency, and the first order moment in frequency to the group delay of the signal. In this study, the first key feature is $\langle \omega \rangle_{t=0}$ and the second one is $\langle t \rangle_{\omega=0}$.

The output from the feature extraction module is an optimal set of features extracted from WVD images that are then fed to the classification module.

2.3. Classification Module

The role of the classification module is to classify or describe observations relying on the extracted features. The classification scheme is usually based on the availability of a set of patterns that have already been classified or described. This set of patterns is termed the training set and the resulting learning strategy is characterised as supervised. Learning can also be unsupervised, in the sense that the system is not given a priori labelling of patterns, instead it establishes the classes itself based on the statistical regularities of the patterns.

The classification scheme usually uses one of the following approaches: template, statistical (or decision theoretic), syntactic (or structural), or neural. In template matching, a template or a prototype of the pattern to be recognized is available. Statistical pattern recognition is based on statistical characterisations of patterns, assuming that the patterns are generated by a probabilistic system. Structural pattern recognition is based on the structural interrelationships of features. Neural pattern recognition employs the neural computing paradigm that has emerged with neural networks.

In our case, a Fisher's linear discriminant is implemented to take care of the last processing step that consists of decision making regarding the defect class. This classifier minimizes the mean squared error (MSE) between the classifier output and the desired labels. It projects high dimensional data onto a line and performs classification in this one-dimensional space. The projection maximizes the distance between the means of the two classes while minimizing the variance within each class. Details about this classifier and other classifiers can be found in [7].

3. Experiments:

The PEC instrumentation used for this work consisted of a pulse generator, a pre-amplifier, an XY positioning robot and a computer-controlled data acquisition system. A schematic of this setup is shown in Figure 2. The driver coil is excited with a 12 volt, 500 μ s long step function triggered upon the probe's arrival at a point of acquisition. The signal is measured as a time-based voltage drop across a resistor in series with the pick-up coil, and fed into a low-noise amplifier. This signal response in the time domain is often called an A-scan. The scanning and data acquisition operations are controlled by the Utex Winspect™ software package. Although the system can accommodate several probe-coil configurations, only the sliding probe arrangement was used in this study. The probe consists of two adjacent coils in driver/pickup configuration.

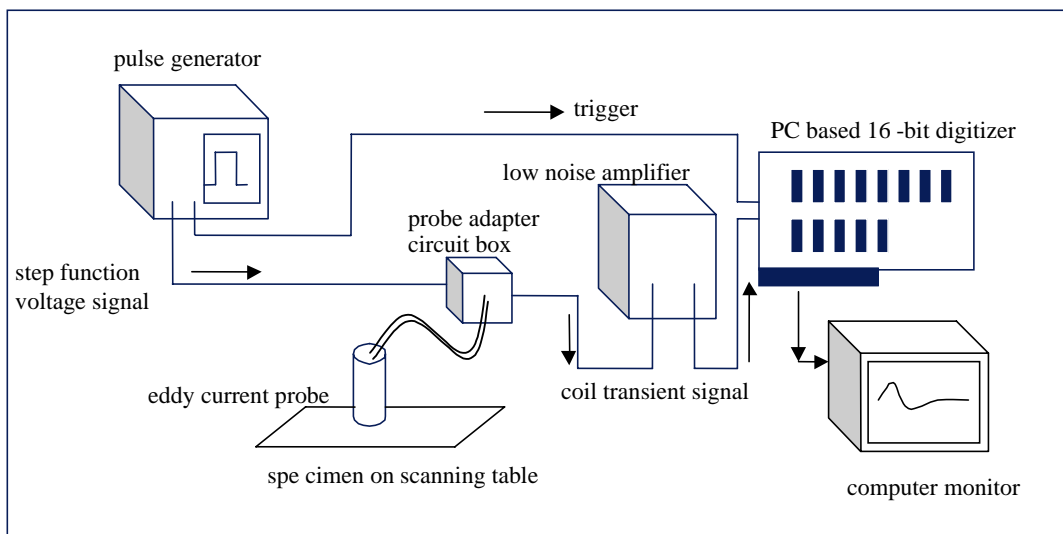


Figure 2: A schematic illustration of the PEC apparatus used in this study.

A test specimen was constructed to simulate a two-layer 0.040"/0.040" aluminium alloy lap splice, as shown in Figure 3. Material loss due to corrosion was simulated by milled areas.

The specimen was scanned at a 1 mm resolution. The signals in each region of interest were captured with 1 MHz sampling frequency. It is the reference subtracted signal, rather than the raw signal, that is analysed when evaluating the condition of the lap splice. The reference signal was taken as the average of all A-scan signals in the region away from flaws. Subsequently, the reference signal was subtracted from those of interest, resulting in a set of reference subtracted signals. These represent the perturbations due to metal loss or other abnormal conditions. Hence forth, these signals will be referred as simple PEC signals.

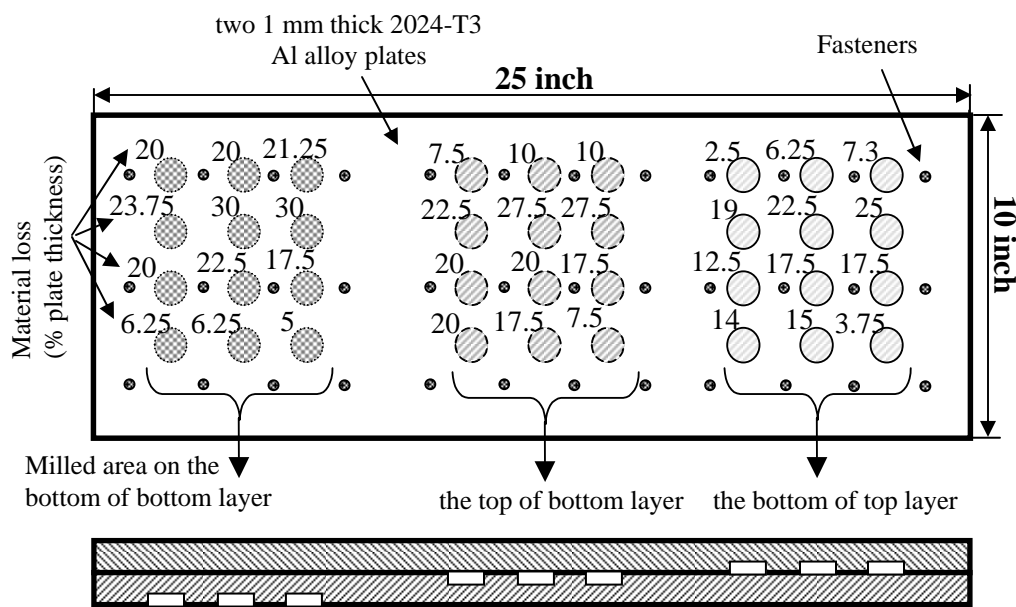


Figure 3: The configuration of the test specimen used in this study.

4. Results and Discussion:

The subtracted defect signatures are fed to the Wigner-Ville Distribution (WVD) computer block to obtain the corresponding WVD images. These WVD images are presented to the feature extractor block for optimal feature extraction. Both feature extractors explained in section 2.2 (PCA and the first order moments of WVD) have been applied to the WVD images and the key features obtained from each extractor have been sent to the classifier separately.

Six different defect classes are considered to test the performance of the proposed method. There are three categories for the location of defects: bottom of top layer (BOT), top of bottom layer (TOB) and bottom of bottom layer (BOB). Each category is divided in two classes: defect with less than 10% of the layer thickness and defect with more than 10% of the layer thickness. The extracted features corresponding to the six simulated defect signatures are fed to the classifier for training. Every training input data is labelled with its corresponding class as indicated in Table 1.

Table 1: List of defect classes and training data set

Defect Class	Training Data
BOT <10%	bot 2.5% & bot 7.5%
BOT >10%	bot 17.5% & bot 25%
TOB <10%	tob 7.5% & tob 10%
TOB >10%	tob 17.5% & tob 27.5%
BOB <10%	bob 5% & bob 6.25%
BOB >10%	bob 20% & bob 30%

The classifier uses these training data to provide the decision boundary. Then, the trained classifier assigns the test data to one of the classes under consideration based on the measured features. Since two different feature extractors were used, the classification process was performed for each of them separately. To get a better sense of the results, the defect classes determined by the classifier for each test data are shown in Figure 4.

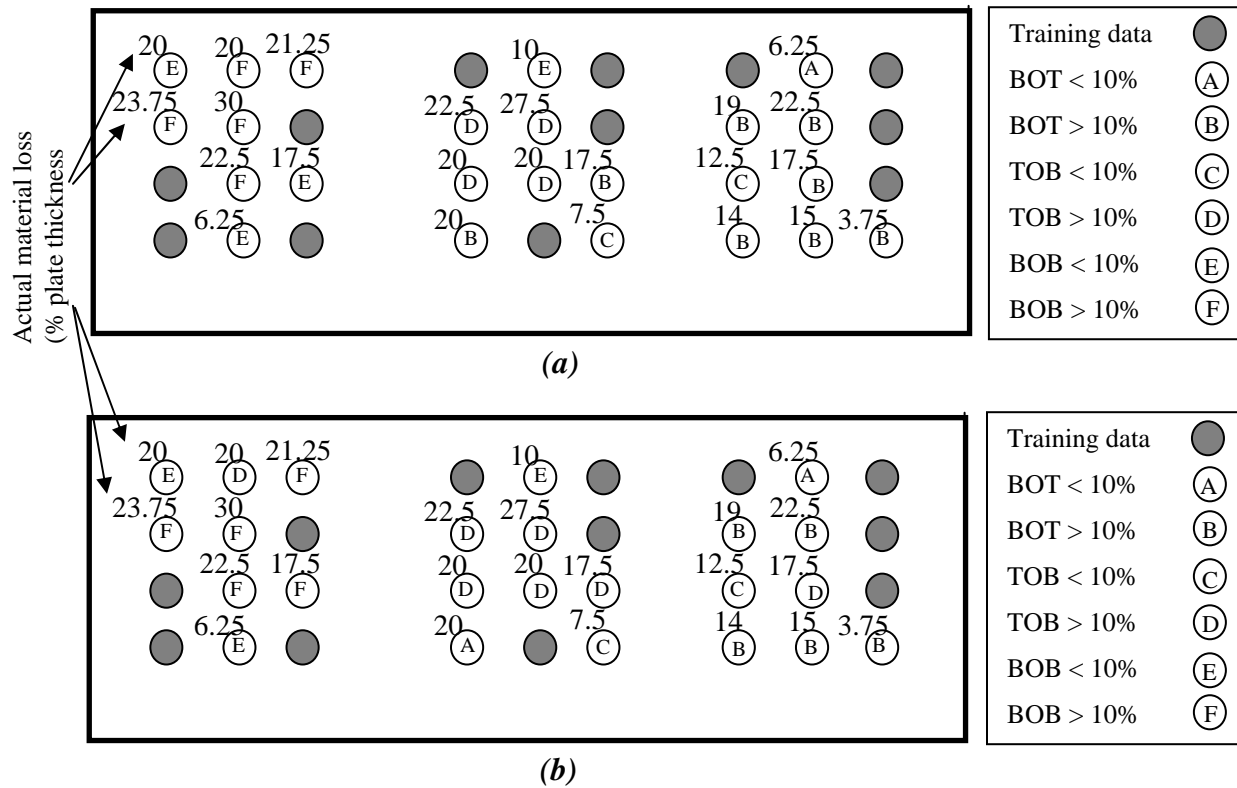


Figure 4: Estimated material loss by classifier using (a) PCA and (b) the first moment of WVD as a feature extractor

Table 2 summarizes the defect classes, the actual material loss and the evaluation for each test data.

Table 2: Comparing actual material losses with defect classes obtained by classifier

Actual Material Loss	Defect Class (using PCA)	Evaluation (using PCA)	Defect Class (using MOM)	Evaluation (using MOM)
BOT 3.75%	BOT > 10%	False	BOT > 10%	False
BOT 6.25%	BOT < 10%	True	BOT < 10%	True
BOT 12.5%	TOB < 10%	False	TOB < 10%	False
BOT 14%	BOT > 10%	True	BOT > 10%	True
BOT 15%	BOT > 10%	True	BOT > 10%	True

BOT 17.5%	BOT > 10%	True	TOB > 10%	False
BOT 19%	BOT > 10%	True	BOT > 10%	True
BOT 22.5%	BOT > 10%	True	BOT > 10%	True
TOB 7.5%	TOB < 10%	True	TOB < 10%	True
TOB 10%	BOB < 10%	False	BOB < 10%	False
TOB 17.5%	BOT > 10%	False	TOB > 10%	True
TOB 20%	TOB > 10%	True	TOB > 10%	True
TOB 20%	TOB > 10%	True	TOB > 10%	True
TOB 20%	BOT > 10%	False	BOT < 10%	False
TOB 22.5%	TOB > 10%	True	TOB > 10%	True
TOB 27.5%	TOB > 10%	True	TOB > 10%	True
BOB 6.25%	BOB < 10%	True	BOB < 10%	True
BOB 17.5%	BOB < 10%	False	BOB > 10%	True
BOB 20%	BOB > 10%	True	TOB > 10%	False
BOB 20%	BOB < 10%	False	BOB < 10%	False
BOB 21.25%	BOB > 10%	True	BOB > 10%	True
BOB 22.5%	BOB > 10%	True	BOB > 10%	True
BOB 23.75%	BOB > 10%	True	BOB > 10%	True
BOB 30%	BOB > 10%	True	BOB > 10%	True

It is clear from Table 2 that in most cases the classifier gives a correct response except when the material loss size is very close to the limit of the class such as 10 or 12.5% material loss. In some cases, the training data do not well represent the classes and are far from the limit of the class. In such a case, the classifier cannot accurately define the boundary of classes.

On the other hand, the results from the two feature extractors used in this study give the same number of false responses. It is very difficult to arrive at a conclusion regarding the performance of these two feature extractors.

There are some error sources that must be addressed. The extractor block only provided two features for each WVD image to permit a visual examination of the data. The PCA analysis can extract more features to better represent the WVD images. In case of the first order moment of WVD, the extraction of the second order moment of WVD can also be interesting to consider because it contains some additional information about the given time-frequency representation. In other words, the loss of information brought on by the PCA analysis or the moment of WVD can be kept at a minimum.

The number of training samples plays an important role in the classification performance. In practice, the error rate of a recognition system is a function of the number of training and test samples. The error rate becomes smaller and smaller as the ratio of the number of training samples per class to the dimensionality of the feature vector gets larger and larger. In this case, there were only two data per class for training the classifier. Despite the small number of training data, the results were good. A large number of training data can significantly improve the performance of the classifier. It is also noted that the classifier approach adopted

in the classification block is the simplest classifier. Using a nonlinear classifier or a neural network classifier may better define the decision boundaries and consequently reduce the error, but they are very sensitive to the number of training data.

5. Conclusion:

In this paper, an automated detection and classification system based on the pulsed eddy current measurements for automatic characterization of material loss in a typical aircraft fuselage multi-layer structure has been developed. The application of joint time-frequency analysis and pattern recognition to pulsed eddy current signals provides an automatic defect classification system and expands the role of the pulsed eddy current technique in the characterization of hidden corrosion in multi-layer lap splice specimens.

6. Reference:

1. Lepine B.A., Wallace B.P., Forsyth D.S., and Wyglinski A., “ *Pulsed eddy current method developments for hidden corrosion detection in aircraft lap splices.*” Proceedings of the 1st Pan-American Conference for Nondestructive Testing, Sept 1998.
2. Bieber J.A., Tai C., and Moulder J.C., “ *Quantitative assessment of corrosion in aircraft structures using scanning pulsed eddy current.*” Review of Progress in Quantitative Nondestructive Evaluation, 17, 1998, PP. 315-322.
3. Safizadeh M.S., Lepine B.A., Forsyth D.S., and Fahr A., “ *Time-Frequency Analysis of Pulsed Eddy Current Signals,*” Journal of Nondestructive Evaluation, Vol.20, No. 2, PP. 73-86, June 2001.
4. Cohen L., “Time-Frequency Analysis,” Prentice Hall, 2000
5. Classen T.A.C.M., Mecklenbrauker W.F.G., "The Wigner Distribution – A Tool for Time-Frequency Signal Analysis", Philips J. Res., 35, 1980, PP. 217-250, 276-300, 372-389.
6. O’Connel M.J., ”Search Program for Significant Variables”, Computer Physics Communications, Vol. 8, No. 1, August 1974.
7. Jain A.K. Dulin R.P.W. and Jianchang M., ”Statistical Pattern Recognition: A Review”, IEEE Transaction on Pattern Analysis and Machine Intelligence, Vol. 22, No. 1, January 2000.

Array Eddy Current for Fatigue Crack Detection of Aircraft Skin Structures

Eric Pelletier, Marc Grenier, Ahmad Chahbaz and Tommy Bourgelas

*Olympus NDT Canada, NDT Technology Development, 505, boul. du Parc-Technologique
Québec (Québec), Canada, G1P 4S9*

ABSTRACT

Fatigue cracks growing rate in an aircraft skin structures is difficult to predict, therefore early detection is very important to avoid structure failure. Small fatigue cracks originating deep in these structures, or in the second layer of the skin and in the region of the fastener holes, are hard to detect using standard driver-pickup eddy current probes. The difficulty lies in the fastener length and spacing, which reduce test sensitivity. This paper explains the development of array eddy current probe and signal interpretation technique designed to detect and visualize fatigue cracks in fasteners holes and at multilayer level.

In this study, an array eddy current probe was evaluated and a new eddy current array coil design is suggested. Several tests were conducted with the developed array on an aircraft lap-joint sample having simulated fatigue cracks. With the improved array design, the results show great potential and enhanced detection capabilities of relatively small size fatigue cracks in fasteners.

1) INTRODUCTION

Airframe manufacturers and airline companies use nondestructive techniques such as eddy current to detect hidden fatigue cracks and skin structure corrosion. With conventional eddy current technique, the basic component is a sensor coil. When the coil is excited by an alternating current and put on or near a conductive material, a resultant eddy current is created on the skin of the material. After the coil passes over a defect, the impedance of the coil will change and this impedance variation is directly illustrated on the screen in a view called the impedance plane (Lissajous). However, such interpretation is not simple task and requires a considerable amount of operator skill and knowledge. A good way to facilitate the interpretation of eddy current signals is to present them in a C-scan view. This kind of representation is made possible with the use of eddy current array (ECA) probes. Furthermore, with the use of ECA probes, a C-scan view can be built with one single of scan, which reduces inspection time tremendously. This paper presents a new ECA probe designed for the detection of deep fatigue cracks which are immediately adjacent to fasteners in relatively thin and multilayered structures.

2) ECA PROBE PRESENTATION

The designed ECA probe represents a transmitter-receiver probe that provides a quick and reliable solution for the detection of fatigue cracks in lap joint structures.

2.1 Transmitter

The investigated ECA probe was first designed and modeled using commercial finite element software (MagNet from Infolytica) to analyze and optimize the probe.

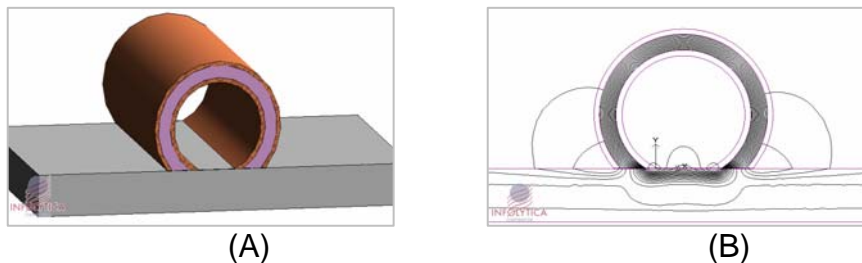


Figure 1: Transmitter coil modeling results

Figure 1 (A) shows the general appearance of the probe transmitter and figure 1 (B) shows the magnetic field distribution produced by the coil. Measurements were made to quantify the produced magnetic field. Such probe configuration provides a powerful transmitter allowing a large magnetic field generation in the inspected material.

2.2 Receiver

The following figure illustrates the configuration of the designed eddy current array probe receiver. The probe is used with an ECA unit (OmniScan), which has an internal multiplexer that activates four pick-up coils at the time. The receiving configuration is composed of 16 coils. Four coils are activated in four acquisition time intervals (or time slots) to activate the complete probe in a very short period of time.

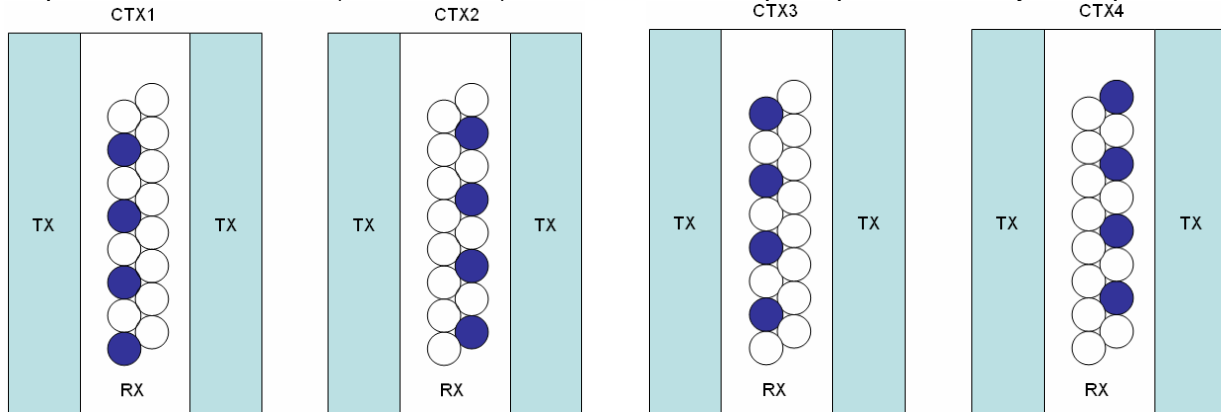


Figure 2: Receiving coil multiplexing

This multiplexing technique provides a large coverage in a single inspection pass while maintaining high scanning resolution. Also, it reduces the need for complex robotics to move the probe; a simple manual scan is often enough when using ECA. R/D Tech (Olympus NDT Canada) was the first NDT instrument manufacturer to use this revolutionary multiplexing technique.

3) SIGNAL INTERPRETAION

This section describes the signals that are produced when the eddy current probe passes over a defect. Figure 3 shows how a C-scan image can be built when an ECA probe passes over a defect. In this case, the coil located just over the flaw produces a strong signal. The further the coil is from the defect, the weaker is the produced the signal. The C-scan view is color coded to represent the amplitude of the close and far coil signals.

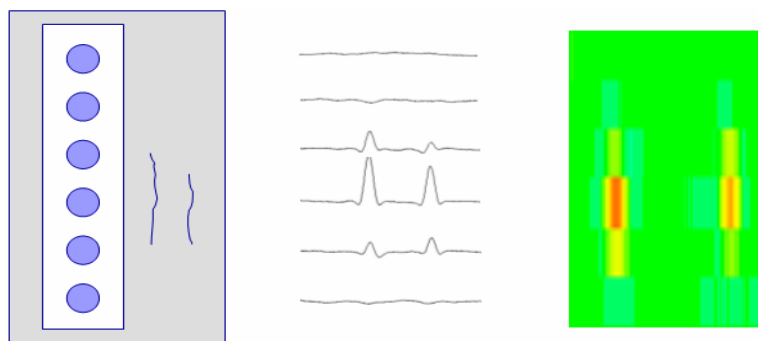


Figure 3: ECA probe C-scan representation

The same principle is used in the inspection of a fastener. When the probe passes over a fastener free of defects, we obtain a signal in the impedance plane as shown on the left of Figure 4. In order to facilitate the interpretation, the signal is rotated until it reaches a horizontal position.

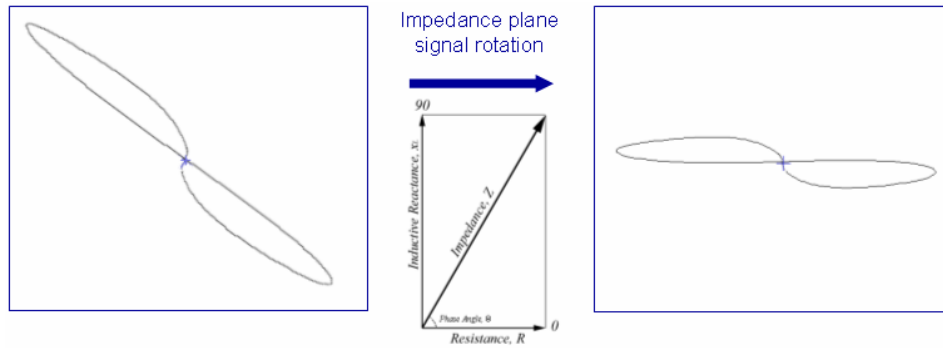


Figure 4: Fastener signal processing

This rotation makes it easy to set an alarm threshold on the Y-axis, which is usually the component affected by a defective fastener (see Figure 5).

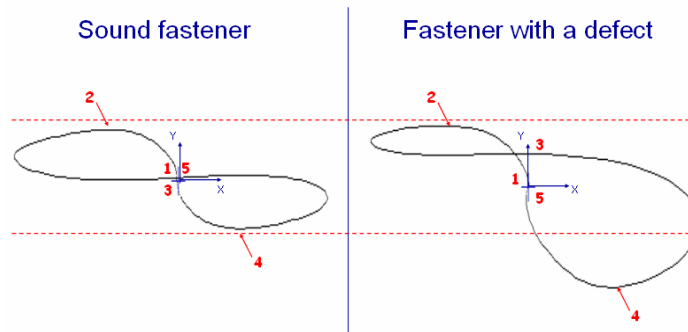


Figure 5: Defect detection signal interpretation

When the probe passes over a fastener with a crack, the signal crosses the alarm threshold and the C-scan of the Y-axis clearly shows the defect. Figure 6 presents the strip chart and C-scan representation of that Y-axis (the X-axis is not used at this moment).

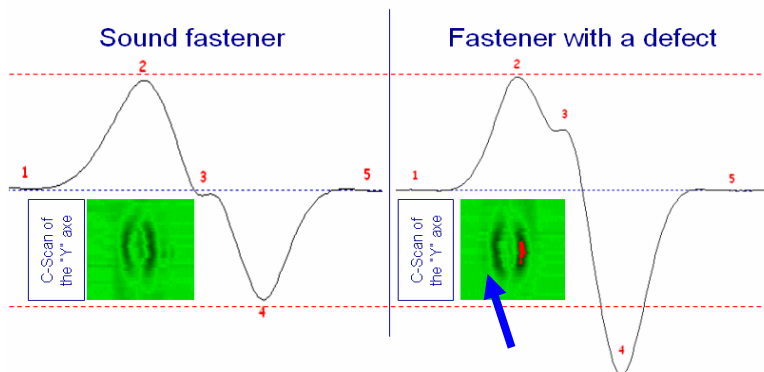


Figure 6: Y-axis strip chart and C-scan signal representation

Each line forming the C-scan represents the measured signal of each receiving coil. It is possible to obtain a smoother C-scan if we use an interpolation processing between each received line.

4) EXPERIMENTAL EQUIPMENT SETUP

The experimental equipment needed for this demonstration is shown in Figure 7. This is a setup built around the user-friendly equipment produced by R/D Tech. The equipment includes the ECA OmniScan unit and software, an ECA probe prototype, and a small position encoder.



Figure 7: Experimental equipment

5) APPLICATION RESULTS

5.1 First experimentation

The first simulated specimen is aluminum machined three-layer thick lap-joint structure. The cracks are located in the third layer of the structure (each layer is 2 mm thick). It is important to mention that such sample configuration represents a considerable thick structure for the eddy current technique. As a matter of fact, the crack is located under 4 mm of aluminum plates.

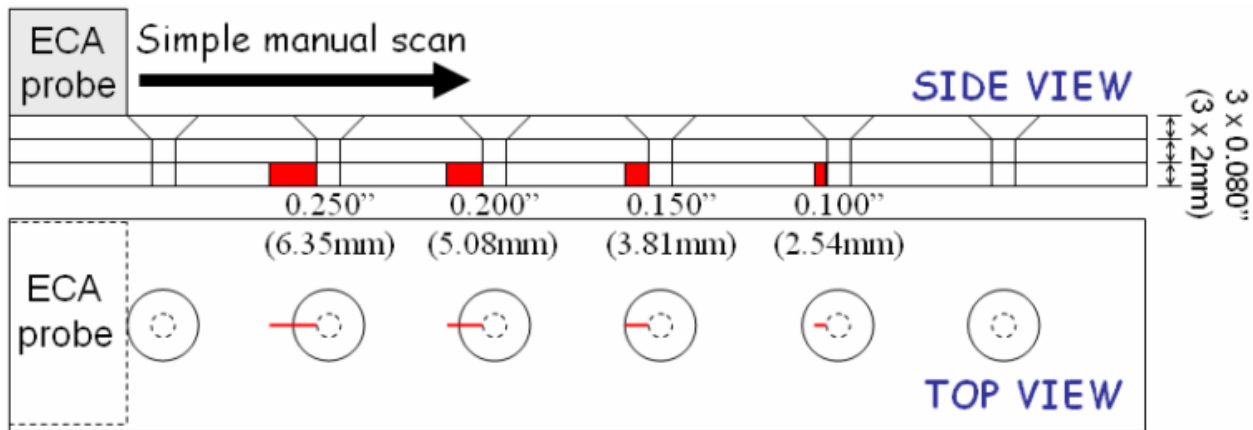


Figure 8: Experimentation 1 configuration

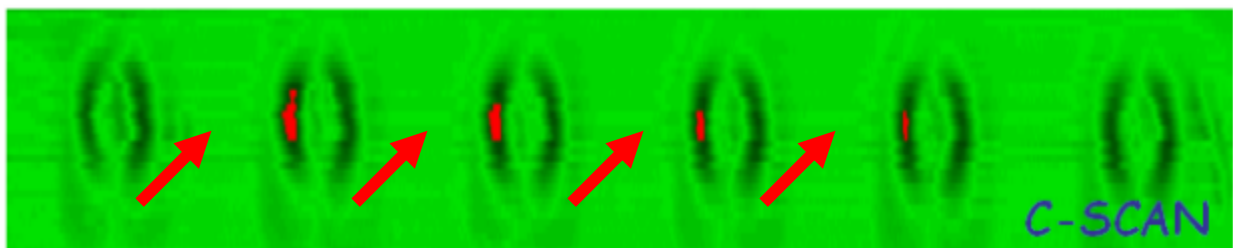


Figure 9: Experimentation 1 C-scan results, frequency of 1 kHz

Scanning with the designed ECA probe, figure 9 shows that we were able to cracks down to 0.100" (2.5-mm) located in the third layer of the simulated lap-joint structure. Another important point is that the ECA probe had very low sensitivity to lift-off.

5.2 Second experimentation

The second application is a machined, three-layer thick lap-joint sample like the first one, but the defects were located in different layers of the structure. Each layer is 1 mm thick.

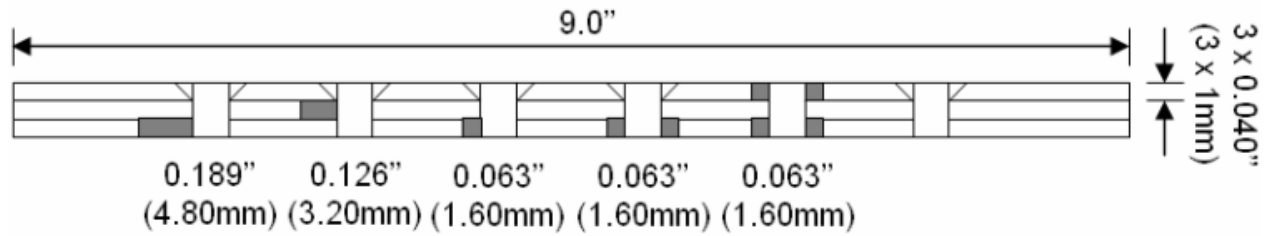


Figure 10: Experimentation 2 configuration

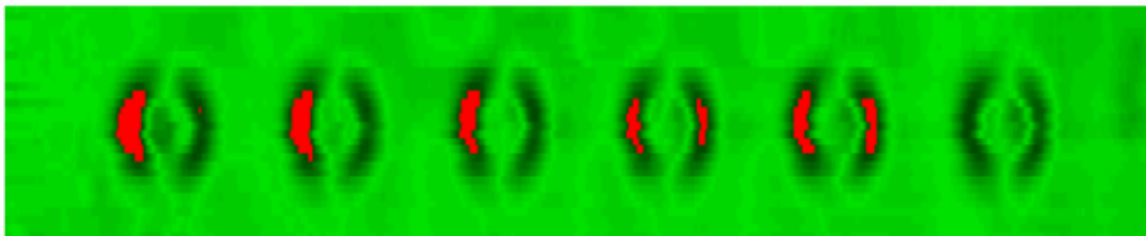


Figure 11: Experimentation 2 results, frequency of 2 kHz

This above results (figure 11) demonstrates that we have been able to detect cracks in the third layer as small as 0.063" (1.6-mm). This setup also allows the detection of defects located in different layers of the structure without any false calls.

5.3 Third experimentation

Figure 12 shows the sample configuration with the different location of the cracks.

Wing Plank Sample (All notches are full thickness)

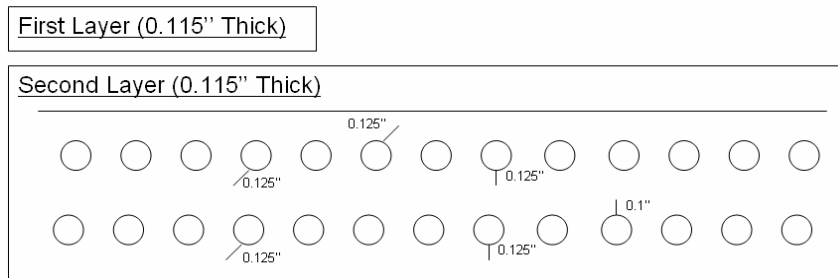


Figure 12: Experimentation 3 configuration

Normally, the fastest way to inspect the plate would be to move the ECA probe along the fastener line. However, since the designed probe has a better sensitivity to the type of cracks oriented along the scanning axis, scanning along the fastener is not really recommended for defects with orientation between 5 and 7 o'clock such the above sample. With such defects, a perpendicular scan or an oriented 45 degrees scan of the fastener line would provide much better results. The following section shows the results obtained for different scan orientations.

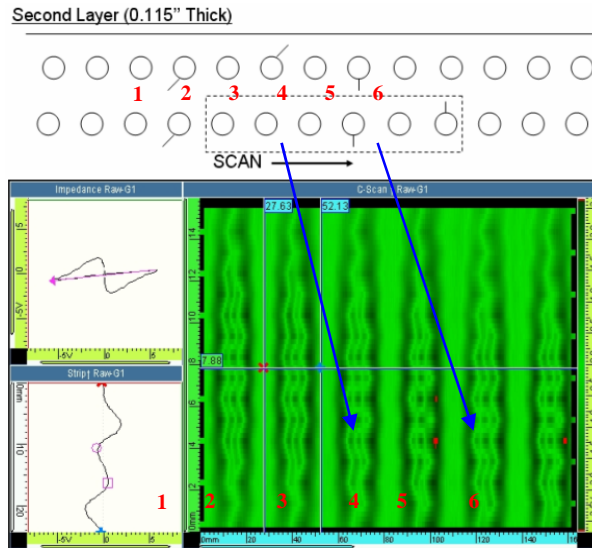
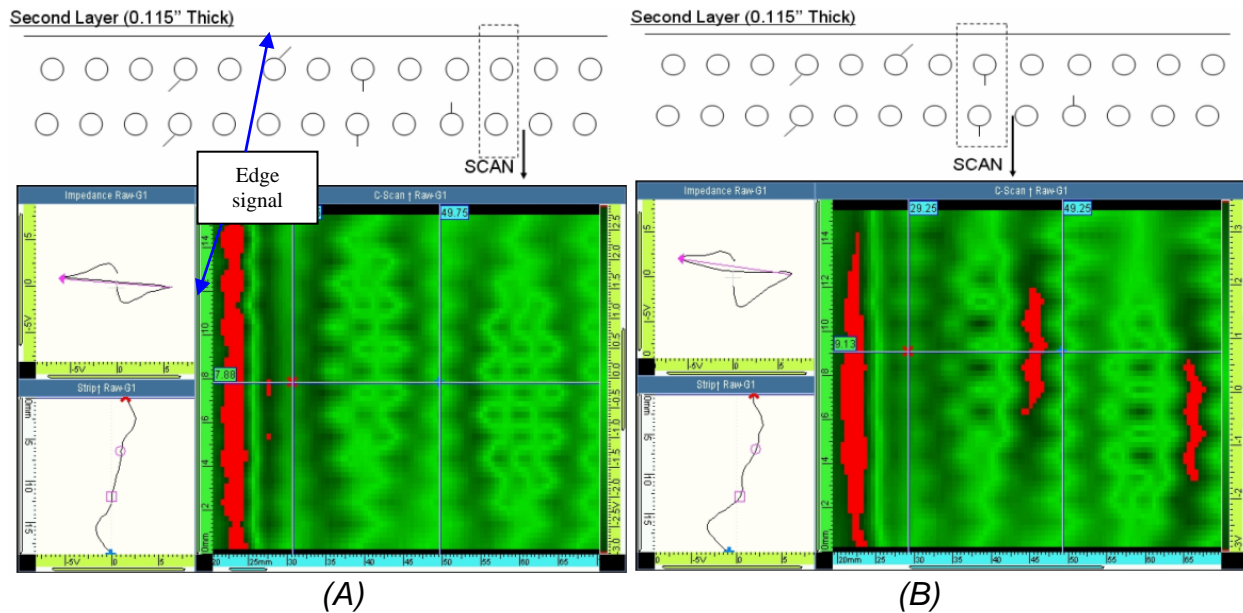


Figure 13: Parallel scan, very weak detection (because of crack orientation)

With the probe moving parallel to the fastener line, it is very difficult to adjust the C-scan color palette to obtain good detection of the cracks. Figure 13 shows two small indications that correlate with the plate defects. However, the signal amplitude that we get from those defects is relatively small and could easily be confused with a good fastener. With this type of parallel scan, the minimum detectable flaw would vary between 0.160"-0.180".



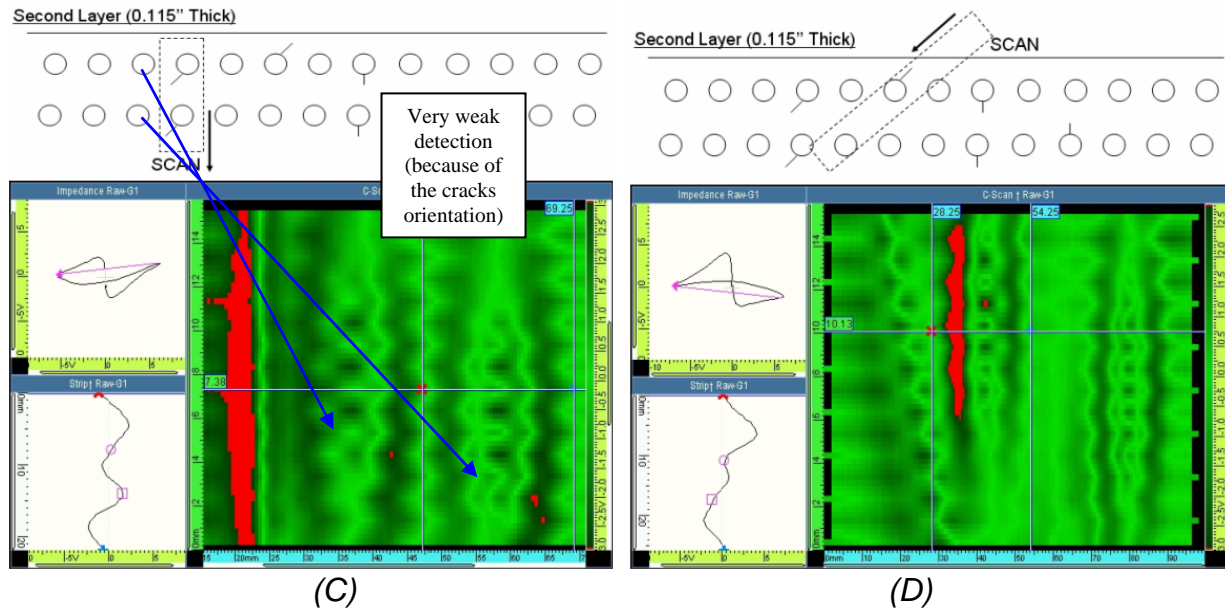


Figure 14: Experimentation 3 Results: frequency of 1.5 kHz – A) Response of good fastener - B) Response for defective fastener with crack at 6 o'clock – C) Response for crack located at 8 o'clock – D) Response for crack located at 8 o'clock (good scan orientation)

When the scan is made perpendicular, the signal response to a crack located around 6 o'clock becomes much stronger. Figure 13 (A) and 13 (B) shows the results from two scans, one made on good fasteners and one made on fasteners with cracks. When the crack is located at 8 o'clock like in the Figure 13 (C), the defective fasteners are more difficult to detect. They can still be detected but the difference with a good fastener response is very small.

Figure 13 (D) shows the scan result for a 45-degree orientation. This type of scan is clearly optimized for defect around 7 and 8 o'clock. The first fastener gives a big signal represented as a deviation in the positive plane of the impedance plane and as an important color change in the C-scan.

To conclude with this third experimentation, the new ECA probe design was able to detect all the fatigue cracks located in the second layer of the simulated lap-joint samples. However, this probe has some limitations:

- A parallel scan can provide very fast scan but the detection level is expected to be more around 0.160" to 0.180".
- Optimum response is obtained when the probe is scanned in the same orientation as the defect. In this case, a crack as small as 0.125 in. can be detected. To cover all direction at this level of sensitivity, a total of four scans are required.

6) FUTURE WORKS

Based on these results, it is possible to confirm that the ECA probe design can be successfully used for fatigue crack detection. However, to be able to obtain a better detection capability, some future work is required:

- Improve the resolution of the probe
- Add real-time calculation of the signal surface inside the impedance plane
- Using modeling for optimization
- Characterize defects and identify their depth using multi-frequency inspection

7) CONCLUSION

In this paper, an ECA probe and practical inspection procedure were demonstrated for fatigue crack detection in multilayered lap-joint structures. The prototype probe showed better detection capabilities compared to the standard ECA probe for crack detection presently on the market. We have demonstrated a very good detection level with a uniform sensitivity on both sides of the fastener. The next steps are: make a standard probe of this prototype and characterize the detection capability with regard to the crack orientation.